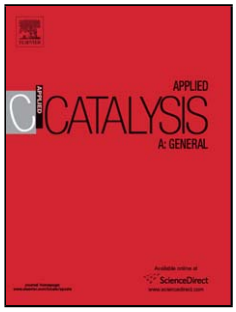

Title: Strong metal-support interactions on rhodium model catalysts

Authors: Ch. Linsmeier, E. Taglauer

PII: S0926-860X(10)00546-6
DOI: doi:10.1016/j.apcata.2010.07.051
Reference: APCATA 12739

To appear in: *Applied Catalysis A: General*

Received date: 16-2-2010
Revised date: 21-7-2010
Accepted date: 27-7-2010

Please cite this article as: Ch. Linsmeier, E. Taglauer, Strong metal-support interactions on rhodium model catalysts, *Applied Catalysis A, General* (2010), doi:10.1016/j.apcata.2010.07.051

Strong metal-support interactions on rhodium model catalysts

Ch. Linsmeier[a,*], E. Taglauer[a]

[a] *Max-Planck-Institut für Plasmaphysik, EURATOM Association, Boltzmannstr. 2, 85748 Garching b. München, Germany*

Abstract

Reactive processes on catalyst surfaces are studied in this work for Rh/metal oxide model systems by means of surface science techniques. Published results in the literature deal with titania, alumina, and silica as support materials and are briefly reviewed. For the present studies Rh/Al_2O_3 and Rh/TiO_2 model catalysts with about one monolayer Rh coverage are specially prepared and analyzed by ion scattering spectroscopy, X-ray photoelectron spectroscopy, and thermal desorption measurements as main techniques. In part these measurements are supported by a variety of other analytical and imaging techniques. For thermal treatment in hydrogen atmosphere at low and elevated pressures a complete Rh encapsulation by titania is observed for temperatures above 773 K. The results from ion bombardment depth profiling are corroborated by the concomitant drastic reduction of the CO adsorption capacity of these samples. The model catalysts thus exhibit the typical features of 'strong metal-support interaction'. The effect was not found for alumina supports, for which thermal treatments mainly resulted in gradual interdiffusion of the various surface species. These results also demonstrate that characteristic catalyst behavior can be successfully studied by applying surface science methods to model catalysts.

Keywords: model catalyst, rhodium, titania, alumina, strong metal-support interactions, SMSI, surface analysis, ISS, XPS, TPD

*Corresponding author

Email addresses: linsmeier@ipp.mpg.de (Ch. Linsmeier), taglauer@ipp.mpg.de (E. Taglauer)

1. Introduction and literature review

1.1. Supported metal catalysts

The activity and selectivity of supported metal catalysts are determined by the choice of the metal, the pretreatment and also by the properties of the supporting oxide. Already G.-M. Schwab discussed electronic interactions between the support and the metallic component, which influence the activation energy and the reaction rate for certain reactions [1, 2]. In this context electronic effects refer to the oxidation states of the substrate which influence the properties of the catalyst. The morphology of the catalyst came into focus by the work of S.J. Tauster et al., who discovered a strongly altered CO and H_2 chemisorption behavior on group 8 metals supported on titanium dioxide (TiO_2), before and after a high-temperature reductive treatment (HTR) in hydrogen at 773 K [3–5]. The term 'strong metal-support interaction' (SMSI) was coined to describe this behavior and was later extended to phenomena which are caused by a high-temperature reduction treatment [6] or generally to changes in the catalytic behavior due to interactions between metal and the non-metallic support [7].

A behavior similar to TiO_2 as a support material was found with other transition metal oxides. The reduction of the CO chemisorption capacity correlates with reducibility of the oxide. Easily reducible oxides such as TiO_2, Nb_2O_5, and V_2O_3 show SMSI behavior, whereas less easily reducible oxides as Sc_2O_3, ZrO_2 or HfO_2 or the main group oxides Al_2O_3 and SiO_2 show no changes in their chemisorption behavior up to 773 K [4]. Electron microscopic observations with Pt/TiO_2 model catalysts showed evidence for the formation of Ti_4O_7 species after elevated reduction temperatures (975 and 1025 K) [8, 9] and gave rise to cluster model calculations [10]. They produced the energetically most favorable results for the assumption of a direct Pt–Ti bond and a formal charge of +3 at the titanium ion. Therefore, the early work about SMSI effects discussed mainly electronic effects, namely the electron transfer from Ti^{3+} to the metal, as the reason for the altered chemisorption behavior [5, 11]. However, the small number of transferred electrons from one Ti^{3+} per metal cluster, being the catalytically active component, is a strong argument against this mechanism as the only reason for the SMSI effect. This was shown by Ray et al. [12] and Spencer [13] for the case of K-promoted catalysts: the electronic effect due to K promotion should be comparable the the influence of a reduced Ti^{4+} species (i.e. Ti^{3+}, Ti^{2+}, ...) and thus have only consequences for the resulting ultimate neighborhood of the promoter atom or the reduced titanium ion. A solution to this dilemma is the encapsulation model, in which the metal is covered

or encapsulated by support material during the transition into the SMSI state. First indications for such an effect were found by Huizinga et al. in X-ray photoelectron spectroscopy (XPS) investigations of rhodium and platinum supported on TiO_2 and Al_2O_3[14]. After a 1073 K reduction of the catalysts the rhodium remained metallic after exposure to air, whereas for lower reduction temperatures, the rhodium was oxidized under these conditions. Also, the reduced H_2 chemisorption of the reduced catalysts is only reversible up to a reduction temperature of 973 K. The different chemisorption properties and the rhodium oxidation behavior were attributed to an encapsulation of the metal particles during the high-temperature reduction (HTR) steps.

The model of a geometric blocking of adsorption sites on the active metal by support oxide is supported by several investigations on inverse systems, in which the oxide is deposited on a rhodium or platinum surface (polycrystalline foil, single crystal) with a coverage of up to approximately one monolayer. The CO chemisorption capacity during these experiments decreased linearly with increasing amount of titanium oxide. This was demonstrated in several experiments: [15–17], and also, with the corrected oxide coverage calibration from [17], in [18–22].

1.2. Titania as support material

Transmission electron microscopy (TEM) experiments with Rh/TiO_2 powder catalysts showed an encapsulation of the metal particles after a 16 h hydrogen reduction at 773 K. [23]. The formed layer has a thickness of 0.2–0.4 nm and shows no structure, in contrary to the supporting oxide. The decreased H_2 chemisorption was not restored by a 2 h oxygen treatment at 473 K and subsequent 16 h reduction at 473 K. However, an extended reoxidation (16 h at 473 K) restored 80 %, and at 773 K, the original chemisorption capacity was completely restored. However, no information about the nature of the encapsulation layer was obtained. With Pt/TiO_2 model systems, also encapsulation effects [24] and reduced support oxide, combined with a Pt–Ti alloying, were reported [25].

Reduced Ti^{4+} was found in experiments which involved rutile (110) single crystals as a support material [26] and evidence for oxide migration was found. These substrates were annealed in vacuum before rhodium evaporation, no oxygen treatment followed the annealing. This was shown to produce an oxygen-deficient surface layer with Ti^{3+} signals in XPS [27]. Therefore, the origin of the detected reduced Ti^{4+} species is ambiguous. The depth profiles, taken with Auger electron spectroscopy (AES) and Ar+ bombardment at 500 eV after HTR at 673 K and also after annealing in

vacuum revealed support material on top of the rhodium layer. Similar results were obtained with model systems consisting of platinum or rhodium, evaporated on a this TiO_2 layer on Ti(0001) single crystals [28–32]. After HTR at 775 K, the hydrogen chemisorption capacity was reduced and SIMS and AES revealed a titanium species on top of the metal (Pt or Rh). From the line shape of the Ti AES signals and the from the O/Ti signal ratio, a reduced Ti^{4+} species was deduced. In comparable experiments with Rh/Al_2O_3 systems, a sintering of the rhodium component above 450 K was deduced from desorption measurements.

XPS and X-ray-induced AES investigations with Rh/TiO_2 model catalysts, consisting of a 4.0 nm oxide layer on a polycrystalline Ti foil, supporting an evaporated Rh film, showed a reduction of Ti^{4+} after a HTR at 773 K as well as after heating in vacuum to this temperature [33]. The same changes are observed with oxide films without a metal overlayer, however much less pronounced. An oxidation at 623 K of the samples after HTR lead to completely restored original sample properties. The author excluded a complete encapsulation of the rhodium by oxide species from the measured Rh intensities.

$Rh/TiO_2/Mo$ model catalysts were studied by Labich et al. [34] using low-energy ion scattering, X-ray photoelectron spectroscopy and thermal desorption spectroscopy. The oxide films grown by chemical vapor deposition on the Mo substrate had a thickness of 10 to 20 nm and showed higher thermal stability compared to those grown by anodic oxidation. A Rh film with a thickness of one monolayer was deposited on top. Heating in ultrahigh vacuum to 670 K resulted in Rh agglomeration followed by encapsulation above 720 K and the formation of reduced titanium oxide species. The observed morphological and chemisorption changes were reversible upon reoxidation and low-temperature reduction, i.e. they exhibited the characteristic SMSI effects.

In contrast to the experiments with model systems or inverse models (oxide on rhodium or platinum), in which often a reduction of TiO_2 was observed, only Ti^{4+} signals are found in real catalysts. All the model systems are similar in their small thickness of the oxide films (of the order of some nm). Moreover, all treatments with the model catalysts are carried out under vacuum or rather low pressures. Defects in the titania of real powder catalysts (impregnated titania powder, metallic rhodium formed by reductive treatment) could be produced by ion bombardment. These defects appear in XPS spectra as Ti^{3+} signals [35]. In contrast to Pt/TiO_2 model systems, where electron diffraction measurements after hydrogen reduction showed Ti_4O_7 [8], this species is not detectable by the same methods with

powder Rh/TiO_2 catalysts [36]. Also no reduced Ti^{4+} species is detectable by XPS at Rh/TiO_2 real catalysts, although electron spin resonance (ESR) and nuclear magnetic resonance (NMR) measurements suggest a $(Ti–H)^{3+}$ species being responsible for the smaller chemisorption capacity in the SMSI state [37]. Ti^{3+} ions are detected in numerous experiments with Rh/TiO_2 real catalysts by ESR measurements [38–42]. However, there is no evidence that the detected Ti^{3+} are located in or near the surface atomic layers of the catalysts. The slow reoxidation of Ti^{3+} ions (several hours in air) is rather an argument for the location of these ions deeper in the bulk of the support material [11]. As a consequence, any Ti^{3+} species present in the bulk of a catalyst, far away from the reactive surface, cannot have any influence on catalytic reactions taking place at the surface of the solid, in the adsorbed phase and in the interaction with species from the gas phase. In several publications, Ti^{3+} is not explicitly detected, but the authors deduced the formation of Ti^{3+} from the blue color of the catalysts after HTR [43, 44]. In conclusion, there is no evidence in the literature that reduced titania species are present at the reactive surface of the catalyst in the SMSI state.

1.3. Alumina as support material

In contrast to Ni/Al_2O_3, the system Pt/Al_2O_3 shows a behavior similar to the SMSI effect on metal/transition metal oxide systems. After a HTR between 773 and 948 K, a strongly reduced chemisorption capacity for H_2 was observed [45, 46]. Similar to the observations in the SMSI cases, this effect cannot be attributed to a sintering of the platinum particles and hence to a reduction of the active surface area of the catalyst. The reduced chemisorption capacity could be restored by an oxidation in O_2 at 753 K, followed by a low-temperature reduction (LTR) in H_2 at 673 K. In the case of thick (200.0 nm) metal films on rutile and sapphire single crystals, a partial encapsulation in combination with a breakup of the metal layer was found with platinum. With rhodium, only on the rutile support material is found on the metal layer after a HTR at 1273 K. After an oxygen treatment at very high temperatures (about 1300 K) an oxidation of the rhodium metal was detected [47]. No agglomeration of the rhodium was observed in Rh/Al_2O_3 systems (1.2 nm Rh on α-Al_2O_3 (0001), pretreated by Ar^+ bombardment and annealing) during HTR at 873 K [48]. On Rh/Al_2O_3 model systems (Al_2O_3 by evaporation of Al onto Mo (110) with O_2 background, oxide layer thickness between 0.6 and 1.0 nm, Rh evaporated with a thickness of around 0.1 nm), encapsulation and diffusion of rhodium into and through the Al_2O_3 was found after heating in vacuum up to 1100–1200 K [49]. The CO chemisorption capacity was lost completely. The formation

of large rhodium clusters during the transition as an explanation for this behavior was excluded in these experiments.

Rh/SiO_2 model catalysts were recently studied by McClure et al. [50], particularly with respect to their characteristics in in low pressure and elevated pressure environments. The systems were prepared under ultra-high vacuum conditions and characterized by a variety of methods, including scanning tunneling microscopy and CO infrared reflection absorption spectroscopy. The number and kind of active Rh surface sites could thus be determined. The results nicely demonstrate the utility of low pressure surface science characterization techniques in understanding elevated pressure reaction kinetics on model catalyst surfaces.

1.4. Present studies

Many aspects of the metal-support interactions, especially the SMSI effects, are intensively studied and well-documented in the literature. Extended reviews are given in [6, 51, 52]. Especially the influence on catalytic reactions has a broad basis of experimental experience. However, the reason of the SMSI effect, be it mere electronic, geometrical or morphological changes of the catalysts during the high-temperature reduction, or a combination of several effects, are discussed differently.

In this work, we assess the interactions between the catalytic metal and the support oxide by experiments with model systems. Such systems are especially well-suited for surface analytical investigations by means of low-energy ion scattering (ISS or LEIS), Auger electron spectroscopy (AES) and X-ray photoelectron spectroscopy (XPS). Thin films produced by oxidation under vacuum conditions, both on single crystalline or polycrystalline metals, are often only a little thicker than the information depth of the applied techniques.

ISS, in combination with slow sputtering of the surface layers, gives information of the elemental composition of the first atomic layers, having a depth resolution within one atomic layer. AES, and especially XPS, give additional chemical information and allow the detection of different chemical states of the elements in the first few atomic layers. To apply these techniques, it is advantageous to have a specimen with a well-defined, flat surface. Also, electrical conductivity is helpful and for some techniques substantial to gain the full information. The model systems studied here are thin oxide films with a thickness of a few ten nanometers, formed by anodic oxidation on a well-polished, high-purity metal foil. These oxide films fulfill both the criterion of sufficient electrical conductivity and also the comparability with real support materials. By anodic oxidation, the properties of

support oxide can be controlled and selected to parallel those of real oxide supports. The metal component is evaporated onto the oxide films under UHV conditions. The dispersion of the metal cluster is also well-defined.

To study the relevance of treatment conditions for SMSI effects, the high temperature reduction were carried out both under vacuum conditions and in an ambient pressure cell. Before using the model catalysts in SMSI experiments, the samples were thoroughly characterized with respect to stoichiometry, thickness, morphology, and crystallinity of the oxide films, as well as with respect to the metal dispersion of the rhodium metal layer. The aim is to study encapsulation effects during SMSI treatments and possible chemical variations in the first atomic layers during the catalyst modifications. Due to the large scope of this work, detailed ISS depth profile measurements on Rh/TiO_2 model catalysts are described separately in an earlier publication [53].

2. Experimental

2.1. Sample Preparation

The model catalysts were prepared on polycrystalline titanium and aluminum foils (Goodfellow, Ti: >99.6 %, Al: 99.999 %). They were polished using a diamond polish with a final grain size of 1 μm and pellon disks. The oxide layer was formed by anodic oxidation with a platinum foil as counter electrode. The natural oxide formed by air oxidation (about 9.0 nm on Al [54] and about 7.0 nm on Ti [55]) was not removed prior to anodization. For both metals aqueous electrolytes were used which do not dissolve the formed oxide layer (Al: 3 % ammonium citrate, $(NH_4)_2C_6H_6O_7$, Merck pro analysi, > 99 %, Ti: 3 % ammonium diborate, $(NH_4)_2B_4O_7 \cdot 4\,H_2O$, Sigma Chemie, $\approx$ 99 %). The current densities were 8 mA/cm^2 in the case of Al_2O_3 and 10 mA/cm^2 in the case of TiO_2, calculated for the front surface of the samples. The current was held constant during the oxidation, which was terminated after the barrier voltage reached values of 10 V (Al_2O_3) and 15 V (TiO_2), respectively. These voltages correspond to alumina and titania thicknesses of about 14.0 nm [56] and 30.0 nm [55]. The formed alumina layers are described as amorphous or γ- and γ'-Al_2O_3 [57, 58]. In the case of TiO_2, the stoichiometric modifications anatase, rutile and brookite, as well as non-stoichiometric phases were observed [55, 59]. However, these different assignments could originate from both, different preparation and examination conditions. All samples were dried in a Simon-Müller furnace at about 390 K for 1–2 hours. The alumina samples were calcined at 823 K for 4 h to provide a complete transformation into γ-Al_2O_3 [60]. Some of the

TiO_2 samples were calcined at 623 K for 4 h where a transformation from amorphous TiO_2 to anatase is expected [61]. The rhodium metal layer with a nominal thickness (calculated for the geometrical sample surface) of about one monolayer (ML) is formed by evaporation under UHV conditions. No prior cleaning procedure is applied. The ultrapure rhodium metal (99.99 %, marz grade) is heated by an electron beam and the evaporation rate of about 0.01 nm/s is monitored by a quartz crystal microbalance during the evaporation.

2.2. Characterization

The samples are characterized using several techniques to ensure the specified properties. The crystal modification of the TiO_2 samples was determined by X-ray diffraction (XRD) and laser Raman spectroscopy (LRS). XRD was performed on a transmission goniometer Siemens type D 500 with Guinier focussing, equipped with a position-sensitive counter [62]. The applied Cu Kα radiation (40 kV, 25 mA) was monochromatized with a Ge(111) crystal. The Raman spectra were recorded using an OMARS 89 triple-monochromator spectrometer (Dilor) equipped with an electrically cooled optical multichannel diode array detector. The instrumental resolution was 5 cm^{-1} and the spectra were corrected for the spectrometer function. Raman scattering was excited by using the 487.9 nm line of an Ar^+ laser (Spectra Physics 2020) with a laser power of about 30 mW. The acquisition time for each spectrum was 16 s.

The oxide film thickness and the metal loading are controlled by ion beam methods (Rutherford backscattering spectroscopy, RBS, and nuclear reaction analysis, NRA) at a 2.5 MeV van de Graaff accelerator. The incident beam direction was perpendicular to the sample surface. The RBS data were collected using a $^4He^+$ ion beam with a primary energy of 1.0 MeV, detecting the backscattered particles under a scattering angle of 165° by a Si(Li) surface barrier detector. The NRA spectra are measured with an incident D^+ beam of 850 keV, using a Si(Li) proton counter with a mylar foil to prevent backscattered particles from reaching the detector. For the determination of the oxide thickness the $^{16}O(d, p_1)^{17}O$ nuclear reaction was used. The cross-section as determined from work of Debras et al. [63] and Amsel et al. [64] is $(5.5–5.7)\cdot 10^{-27}$ mb/sr. To convert the number of oxygen atoms into a layer thickness, the densities $\rho = 3.4$ g/cm^3 for γ-Al_2O_3 and $\rho = 3.84$ g/cm^3 for anatase are used. For the rhodium metal, a density of 12.40 g/cm^3 is used [65].

The morphology was controlled by microscopic techniques (transmission electron microscopy, TEM, scanning force and scanning tunneling mi-

croscopy, AFM and STM).

2.3. In situ low pressure experiments

The experiments at low pressures were carried out in the UHV chamber DESPERADO. The main chamber has a base pressure of $1–2 \cdot 10^{-11}$ hPa and is equipped with a loadlock for sample exchange. Up to five samples are mounted on a transferable support which also holds NiCr/Ni thermocouples and the corresponding contacts. The thermocouples are spotwelded on the sample surface to ensure an optimum thermal contact. The samples can be heated by electron impact from the back. Tungsten filaments are mounted in several positions in the chamber for this purpose. Electrons emitted from the incandescent wires are accelerated towards the sample by high voltage up to 1200 V. In situ gas dosing is possible through a gas shower, consisting of a glass capillary array at a distance of several millimeters from the front of the sample surface. The pressure at the sample surface during the dosing is estimated to about 10^{-4} hPa, depending on the pressure in the gas inlet system [66]. For the experiments described here, ultrapure hydrogen, oxygen and carbon monoxide (glass bottles, 99.999 %) are used.

The chamber is equipped with two single pass cylindrical mirror analyzers (CMA, scattering angle 137°) for ion scattering spectroscopy (ISS, 3M 515) and Auger electron spectroscopy (AES, Varian 981). Both, the ion and electron guns are mounted coaxially inside their CMA. The sample normal is tilted by 30° with respect to the CMA axis. Thermal desorption spectroscopy (TDS) and residual gas analysis are performed using a quadrupole mass spectrometer (UTI 100C, later Hiden HAL 3F/301). The ionization system of the quadrupole mass analyzer is equipped with an entrance shield to preferably detect species originating from the sample surface during the desorption experiments.

Ion scattering spectra are measured with $^4He^+$ ions at an incident ion energy of 500 eV and a current density of about 2 $\mu A/cm^2$. The beam diameter is approximately 0.5 mm. The same ion beam is used for ISS and sputter-etching of the model catalysts. For a recent review of the method, see [67]. Since the beam is well defined and the beam spots are visible in the secondary electron image, several treatments and subsequent depth profiles can be carried out on one sample without mutual interference. Although the beam spot has a Gaussian profile (determined by scanning the beam over a 0.5 mm diameter Faraday cup), the profile influence on the depth profiles was negligible. This was determined in separate calibration experiments with well-defined surface layers. The ISS depth profiles are extracted from the peak integrals of a sequence of ISS spectra. For that reason, Gaussian-type

functions were fitted to the peaks in the ISS spectra, taking the background into account by a linear function [68]. The integrals are plotted versus the ion fluence accumulated up to the beginning of the respective spectrum. With the valid assumption of a constant sputtering yield, the depth eroded by the ion beam is proportional to the ion fluence. However, since the model catalysts are a heterogeneous system, the sputtering yields of pure materials are not straightforwardly applicable. For the case of the rhodium model catalysts supported on titania and alumina, a fluence of $3–6 \cdot 10^{16}$ He^+ cm^{-2} is estimated for eroding one monolayer [69, 53].

The titania and alumina supported model catalysts were subjected in situ in the UHV chamber to reduction treatments at increasing sample temperatures between 470 and 870 K, applying a hydrogen partial pressure of about 10^{-4} hPa to the front of the sample. The gas dosing was established before heating the sample at the respective temperature in 30–60 s and holding it for 15 min. The reaction gas was dosed until the sample temperature dropped at least below 450 K. Each step in these three experimental series was characterized by AES, carried out directly after the sample had cooled down to room temperature after the treatment, and an ISS depth profile.

2.4. Ambient pressure experiments

The Rh/TiO_2 model catalysts were reduced at ambient pressure in a reaction cell at temperatures between 600 and 820 K. The reaction cell was attached to the UHV system and the samples were transferred into the UHV chamber for X-ray photoelectron spectroscopy (XPS) analysis without contact to the air. The reduction was carried out with dilute hydrogen (5 % H_2 in nitrogen, both Linde 5.0, dried in Oxysorb cartridges) or pure hydrogen, for 15 and 30 min, depending on the experiment. During the reductions a constant gas flow was maintained (about 50 cm^3/min). Before the temperature treatment and after the reduction, the atmosphere in the cell was exchanged by flowing about 10 times the cell volume of reaction gas or pure nitrogen through the setup.

XPS analysis was carried out using Mg Kα radiation (1253.6 eV) and a hemispherical analyzer (VSW HAC 100). The base pressure of the XPS chamber was 10^{-9} hPa. The spectra were recorded in the fixed analyzer transmission (FAT) mode with a pass energy of 22 eV. Data points were measured for 0.2 s every 0.06 eV and spectra were accumulated 30–50 times to improve the signal-to-noise ratio. The C 1s signal of ubiquitous carbon was measured before and after every measurement series and was used for the energy calibration with a value of 285.0 eV, found in several experiments

[70–72]. A commercial software (VSW) was used for the spectrum evaluation. The X-ray satellites were calculated from the signals and subtracted. Depending on the signal, a linear, integral, or a background with consideration of the inelastic scattering after Shirley [73] was subtracted. To check for reduced titanium species (Ti^{3+}, Ti^{2+} or lower) besides the Ti^{4+} signal from TiO_2, the Ti $2p_{3/2}$ and $2p_{1/2}$ signals were fitted with a sum function of Gaussians and Lorentzians [74]. The criterion for the quality of the fit was the reproduction of the experimental data points by the fit function. The theoretical area ratio of the doublet split by spin-orbit coupling was considered, however not strictly enforced during the fit procedure, since it is influenced both by the selected background subtraction procedure and final state effects like shake-up satellites, which overlap partially with the photoelectron peaks [75].

3. Results and discussion

3.1. Sample characterization

Before using the model catalysts for SMSI experiments, the thickness of the oxide layer, the metal adlayer and the morphology of the oxide layer, as well as the crystallographic modification of the formed oxide were examined. The thickness of the oxide film depends both on the anodization voltage and on the subsequent treatment. Table 1 shows some typical values of several model catalysts, measured by NRA. The experimental values are compared to the nominal values, which were expected from the preparation conditions. The oxide film thickness is calculated with an average NRA cross section of $5.6 \cdot 10^{-27}$ mb/sr and the densities mentioned in section 2.2. In the case of the alumina, the actual thickness is larger than the expected value. This was already observed in a previous work, where it was also shown that the anodically grown oxide film exhibited a gradient of decreasing oxygen content towards greater film depths. Only the first several atomic layers of the oxide are stoichiometric Al_2O_3. The alumina layer is extended by the calcination treatment [69].

For TiO_2, Table 1 shows that the oxide thicknesses obtained after the anodization and drying are smaller than expected. As in the case of Al_2O_3, the thickness of the oxide films increases during the calcination of the samples. In contrast to the Al_2O_3 films, where XRD did not show any signals originating from the oxide layer, with TiO_2 the modification of the oxide films could clearly be resolved. Without a calcination treatment, no oxidic modification is visible, indicating the amorphous character of the oxide. After a calcination at 623 K, the oxide is converted to anatase. Fig. 1 shows

diffraction patterns of 30.0 nm and 300.0 nm TiO_2 films. In both cases, anatase signals are clearly visible besides the diffraction peaks originating from the underlying Ti metal. The anatase signals become stronger after a 770 K calcination, indicating a growth of the oxide film thickness. After this treatment, also a very weak diffraction peak, probably originating from a rutile contribution, is detected. Laser Raman spectroscopy confirms the transition from an amorphous titania film to an anatase structure during the calcination procedure, as is shown in Fig. 2. Panel a is the spectrum measured at a 30.0 nm thick titania film after drying. No peaks besides the calibration signal at 1057 cm^{-1} are observable. However, even after the 770 K calcination, no rutile is detectable. Fig. 2b shows the spectrum of a thin film with a nominal thickness of 30.0 nm after calcination. Such films are used in the SMSI experiments. Only signals originating from the anatase modification are visible. Fig. 2c shows the Raman spectrum of a 300.0 nm film. Due to the larger film thickness, the signals in this spectrum are much stronger. However, even the thick oxide film exhibits only the characteristic signals for anatase, no rutile modification or signals due to reduced titanium oxides (like Ti_2O_3) [76, 77] are visible.

The thickness of the rhodium metal overlayer is determined by RBS. Since rhodium is the heaviest element in the model catalysts, its amount can be determined with high accuracy. RBS is used to compare the absolute rhodium loading with the nominal thickness, monitored by the quartz microbalance during the evaporation process. As can be seen in Table 2, the measured rhodium layer thicknesses do not match the nominal values. This means that the thickness control using the quartz crystal microbalance has to be used with care. The consistently low values of deposited Rh layer thicknesses are probably due to a calibration error in the quartz crystal microbalance. Loss of rhodium during the sample preparation is unlikely due to the low applied temperatures compared to the Rh melting temperature (2237 K). Nevertheless, the rhodium is uniformly distributed over the model catalysts. The calculated thickness for a TiO_2 film without a rhodium adlayer allows to an estimate for the precision of the method. The mean value of 0.03 ML rhodium for this sample is calculated from the small background in the region of the rhodium peak.

3.2. In situ low pressure experiments

In the experiments carried out in the UHV chamber DESPERADO the samples are submitted to several treatments at different temperatures. The analysis is performed by ISS and depth profiling as well as AES. ISS in conjunction with slow sputtering allows the detection of a possible encapsulation

during sample treatments, even on a atomic layer level. AES is a second method available, however, it has a less pronounced first layer sensitivity than ISS.

3.2.1. Titania as support material

The ISS depth profiles clearly prove that during the HTR treatment the rhodium layer of the Rh/TiO_2 model catalysts is encapsulated. Fig. 3 shows the depth profiles after reductive treatments at 573 and 773 K, respectively, in view of the Rh, O, and Ti intensities. The depth distribution of the rhodium fraction in the first monolayer of the model catalyst changes significantly. At the lower temperature, the rhodium is located in a layer at the surface. The rhodium fraction drops with increasing ion fluence due to sputtering within the first $12 \cdot 10^{16}$ He^+ cm^{-2}. After the 773 K HTR, the first layer is strongly depleted in rhodium. At about the depth of one monolayer ($3 \cdot 10^{16}$ He^+ cm^{-2}), the rhodium fraction shows a maximum and drops subsequently. These changes in the composition of the first layers of the model catalyst can be interpreted as a change in the morphology where the rhodium adlayer is covered by a layer in the monolayer range during the HTR treatment. This change is also reflected in the oxygen and titanium signals. Before the encapsulation takes place, the first atomic layer is both depleted in oxygen and titanium, compared to the deeper layers. After HTR at 773 K, the encapsulated Rh layer leads to a minimum in both the O and Ti signals. These results indicate that the first layer of the model catalyst consists of rhodium islands which cover a large fraction of the surface. However, the rhodium does not form a continuous layer, since there is still oxygen, and in particular also titanium, visible in the ISS spectra.

The encapsulation of the rhodium adlayer during the HTR treatments with increasing temperature is reflected in the increase of the Ti/Rh intensity ratios, both in ISS and AES measurements, shown in Fig. 4. The ISS data is taken after an ion fluence of $3 \cdot 10^{16}$ He^+ cm^{-2}, representing the composition of the surface after sputtering of approximately one monolayer. The AES data is the ratio of the Ti LMM and the Rh MNN signals, thus averaging over a depth of several atomic layers. Initially, the AES ratio is smaller than the ISS ratio, since the AES information depth is larger and the contribution of the Rh signal stronger. After onset of the encapsulation process (773 K, as shown above in the ISS depth profiles of Fig. 3), both ratios are similar. This indicates that after this reduction the depth distributions of the two metals are similar. With both techniques, the change in the surface composition can be detected. However, the proof for encapsulation of Rh by titania species is directly seen in the ISS depth profiles.

As summarized in section 1, the reduction of the CO chemisorption capacity is discussed in the literature as a characteristic indication of the SMSI effect on supported catalysts. The encapsulation of the active rhodium component leads to a destruction of the active sites which are also responsible for the adsorption of CO on rhodium. This is tested at the Rh/TiO_2 model catalysts by exposure to CO and subsequent thermal desorption measurements. Fig. 5 shows TDS spectra from an untreated sample (after a gentle cleaning procedure which is necessary to remove adsorbed contaminants from the air transfer) and after a HTR at 830 K. The cleaning involves dosing of O_2 with a partial pressure of about 10^{-4} hPa at a sample temperature of 573 K. A subsequent AES measurement shows a strongly reduced carbon intensity. The cleaned Rh/TiO_2 model catalyst is exposed to 40 L of CO at 300 K. The measured TDS spectrum can be approximated by two Gaussians which yield desorption energies after a Redhead analysis (first order desorption, $\nu = 10^{13}$ s^{-1}) [78] of 0.98 and 1.12 eV. A variation of the CO exposure between 0.25 L and 40 L shows that the 1.12 eV desorption state is populated almost exclusively up to CO doses of 1 Langmuir. This state is described in the literature as an on-top CO adsorption state [79, 80]. The 0.98 eV desorption state is populated only after saturation of the on-top sites and is described as a bridge position.

After a 830 K HTR treatment the Rh/TiO_2 model catalyst looses the CO adsorption capacity completely. The lower TDS spectrum in Fig. 5 shows only the baseline of the mass spectrometer and a slightly rising background. The steps at 340 and 530 K are a artifacts from the signal amplifier range switching. After the reductive treatments all CO adsorption sites are no longer present and no desorption signal is measured. Therefore, no more CO adsorption sites are available on the Rh/TiO_2 model catalyst in the encapsulated state.

3.2.2. Alumina as support material

Rh/Al_2O_3 model catalysts are investigated after reductive treatments with H_2 up to 823 K. The ISS rhodium depth profiles after 603, 753, and 823 K are shown in Fig. 6 for a model catalyst with a nominal Rh loading of 1 ML. The changes in the Rh depth profiles after these HTR steps are less pronounced compared to the observations at the Rh/TiO_2 model catalysts and the peaking of the Rh fraction at small fluences is absent. After the 603 K step, the Rh signal evolution is compatible with a metallic Rh layer which is not covering the supporting oxide completely. After an initial steep decrease up to $5 \cdot 10^{16}$ He^+ cm^{-2} the Rh intensity decreases with a slower, linear rate. This indicates that the film morphology is not simply a stacking

of layers or islands, however, the precise geometry cannot be determined from this data. Erosion of the overlayer with an ion beam does not result in an idealized 'peeling off' layer by layer, i.e. bombardment induced mixing and effects of the beam profile can also contribute to the residual Rh signal. In comparable reduction treatments of Rh/TiO_2 model catalysts XPS measurements show a complete reduction of the Rh to the metallic state, which can also be assumed for the Rh/Al_2O_3 model catalysts. The next reduction steps at 683 K (not shown) and 753 K show similar rhodium depth profiles with a linear decrease over the whole fluence range. This indicates that the dispersion of the Rh film is lower than before. It is known from the literature that Rh dispersion on alumina substrates is strongly dependent on the precise alumina phase [81]. After the 823 K HTR step the Rh depth profile changes again and exhibits now a small maximum. However, this maximum is much less pronounced than for the Rh/TiO_2 model catalysts (see Fig. 3). Since also no minima are visible in the corresponding Al and O depth profiles (not shown, only in the Al profile a slight depression, much less pronounced than for the Rh signal, is measured), an encapsulation of the Rh by support material comparable to the titania case can be excluded. For the Rh/Al_2O_3 model catalysts, the development of the depth profiles with increasing reduction temperature can be explained by partial covering due to diffusion of Rh into the substrate, combined with an increasing broadening of the Rh depth distribution.

3.2.3. Driving force for encapsulation

Under all treatment conditions applied here to the Rh/TiO_2 model catalysts, an increase of the Ti/Rh ration is observed above 750 K, indicating a thermally activated process. An empirical description of the mobility of a surface species is the Hüttig temperature, defined as 1/3 of the melting temperature [82]. Rutile has a melting point of 2173 K, resulting in a $T_{\text{Hüttig}} = 724$ K. This corresponds to the observed encapsulation temperature, which results in a monolayer of oxide on top of the rhodium in case of TiO_2. Al_2O_3 shows a much weaker effect and only a weak maximum in the Rh ISS signal is observed after the 823 K reduction step. The melting point of Al_2O_3 at 2327 K leads to a $T_{\text{Hüttig}} = 775$ K. Energetically, the free surface energy of the involved components can be discussed [82]. Thermodynamically the spreading of one phase over another is feasible if the free surface energy decreases during this process ($\Delta F = \gamma_{ag} - \gamma_{sg} + \gamma_{as}$, a denoting the adsorbate, s the substrate and g the gas phase). Although the interface energy γ_{as} is unknown in most cases [82], the tabulated values for γ_{ag} and γ_{sg} allow an estimation of the spreading behavior. The values Rh are

275 μJ cm^{-2}, for TiO_2 between 28–38 μJ cm^{-2}, and for Al_2O_3 between 65–93 μJ cm^{-2} [83, 84]. In our case, rhodium acts as substrate and the oxides as adsorbates. Given a sufficient mobility above the Hüttig temperature, these energy values suggest a spreading of the titania above the rhodium. For alumina, the energetic conditions are less favorable for spreading, therefore explaining at least qualitatively the different observations for TiO_2 and Al_2O_3 as support materials.

It is worth noting that the SMSI effect is not observed under oxidizing conditions. Under these reaction conditions, however, the metal component is also at least partially oxidized, therefore the surface free energy difference to the support oxide becomes less pronounced. As a consequence, the driving force as discussed above is diminished. As shown in an earlier publication [53] a high temperature oxidation treatment does not reverse the encapsulation.

3.3. Ambient pressure experiments

The experiments at ambient pressure and subsequent analysis by XPS aim to prove whether reduced Ti^{4+} species (namely Ti^{3+}, Ti^{2+} or lower oxidation states of titanium) contribute to the encapsulation process. Since it could be shown in the low pressure experiments that AES is capable of detecting the encapsulation of the rhodium layer, XPS with the same information depth is able to provide the same information. XPS moreover has the capability to distinguish between the different oxidation states of the elements.

To prepare for the reduction experiments with the Rh/TiO_2 model catalysts, the sensitivity of XPS in the given experimental setup to detect Ti^{3+} was tested. For this purpose, a 30.0 nm TiO_2 film was bombarded with Ar^+ with an incident energy of 2 keV in several steps with increasing fluence. By this treatment, defects can be produced in a titania surface which results in a local decrease in the oxidation state of the Ti^{4+} [85]. Before ion bombardment, the only detectable Ti species in the Rh/TiO_2 model catalyst was Ti^{4+}, as is shown in Fig. 7a. After an ion fluence of $1.11 \cdot 10^{16}$ Ar^+ cm^{-2}, Ti^{3+} was detected as a second signal in the XPS Ti 2p spectrum, shown in Fig. 7b. In the case of the bombarded sample, the experimental data points could be fitted by only two doublets, representing signals from Ti^{4+} and Ti^{3+} within the detection range of XPS. To estimate the sensitivity of XPS for Ti^{3+} in the first layer of the model catalyst, Ti 2p signals with a different amount of Ti^{3+} were calculated, as shown in Fig. 8. The bottom panel shows a measured Ti $2p_{3/2}$ signal (circles), together with a best doublet fit (lines).

In the plots above, the signal intensities were calculated for given amounts of Ti^{3+} (with respect to Ti^{4+}). From Fig. 8 it can be deduced that in the detection range of XPS a Ti^{3+} fraction of about 1.5 % could be recognized with the fitting procedure. This signal is taken as the detection limit for Ti^{3+} with XPS for the model catalysts. Taking into account the inelastic mean free paths for electrons with an energy of 800 eV in TiO_2, namely 2.83 nm after Seah and Dench (SD) [86, 87] and 1.60 nm after Tanuma, Powell and Penn (TPP) [88–90], the contribution of the first atomic layer to the total signal intensity can be calculated. For an electron exit angle of 35°, under which the spectra in Fig. 7 and 8 were measured, the first layer must consist of 11.2 % and 6.8 % Ti^{3+} for the SD and TPP values, respectively. Calculated for the electron exit angles of 20° and 60°, at which the measurements at the Rh/TiO_2 model catalysts during the reduction experiments were carried out, the detection limits are 12.8 % and 7.4 %, respectively, for the SD case and 7.6 % and 4.4 % in the TPP case. These arguments hold for ideally flat surfaces only. For rough real surfaces, these numbers can only be approximations, since on the one hand the number of exposed surface atoms is increased and on the other hand, the morphology of the surface in connection with the detection angle can lead to attenuation effects. In principle, there are also ways to derive oxidation states of surface metal species from ion scattering data [91]. However, the required data from, e.g., adsorptive N_2O decomposition were not available in our case.

During the ambient pressure experiments using Rh/TiO_2 model catalysts with a nominal rhodium metal loading of 1 ML, two treatment series were carried out. The first series starts with a hydrogen concentration of 1.5 % in the reaction gas at temperatures of 603 K, 683 K and 753 K, held for 15 min, and subsequent treatments in pure hydrogen at temperatures of 683 K (30 min), 753 K (65 min) and 823 K (30 min). The second series starts with 15 min treatments in 5 % hydrogen in nitrogen at the temperatures 603 K, 683 K and 753 K. Subsequent treatments at 753 K (15 min) and 823 K (47 min) were carried out in pure hydrogen.

The Rh 3*d* signals for the first series are plotted in Fig. 9. The spectra are the raw data after subtraction of the X-ray satellites. The vertical line marks the Rh 3*d* peak positions, determined after background subtraction and data fitting with Gaussian/Lorentzian functions. The rhodium signal is shifted to lower binding energies already after the first hydrogen treatment. The same effect was observed in the second series with a larger hydrogen fraction in the reaction gas. Additionally, the peak width decreased after this reduction step. The peak positions and widths for all signals of the two treatment series are summarized in Tab. 3. The photoelectron signals at

308.8 eV and 308.9 eV of the untreated model catalysts can be attributed to Rh^{3+} in Rh_2O_3 [92–94]. The evaporated rhodium exists as Rh_2O_3 before any further treatment. However, the large width of the peaks is caused by rhodium in several different chemical environments and shows that the rhodium oxide is not very well defined.

Already a very soft reductive treatment was sufficient to transform the oxide into rhodium metal. The binding energies after the reduction agreed well with the values for rhodium metal in the literature, which lie in the range of 307.0 to 307.5 eV [92, 95–97]. In addition to the shift after the first treatment, after all further treatments the Rh 3*d* signals moved by 0.1–0.3 eV. In the first treatment series, all shifts trended towards smaller binding energies, whereas in the second series the direction is not unequivocal. Shifts of a few tenths of an eV were also observed in the peak positions of the Ti 2*p* signals. These shifts are attributed to experimental uncertainties and to the fact that the binding energies are referenced to the position of the C 1*s* signal measured with every spectrum series. This normalization is also responsible for the shift of the Ti 2*p* signals to higher binding energies after the first sample treatment. It is observed in both treatment series, as can be seen in Tab. 3. A change in the oxidation state of the titanium atoms as a cause for this shift can be excluded, since the whole Ti doublet is affected. This would only be possible if all Ti atoms in the detection range for XPS changed their oxidation state, since the doublet can be fitted with only two Gaussian/Lorentzian functions in the spectra of the untreated and the reduced sample states. The C 1*s* shift as a reason for the peak shifts after the first reduction is also supported by the fact that the measured Rh 3*d* binding energies lie at the upper limit within the range of the literature values. The shift to higher binding energies due to the change in the C 1*s* reference signal also affected the O 1*s* peak and lead to a 0.2 eV shift in both treatment series after the first reduction step.

Despite the shift due to the carbon reference signal no significant changes in the Ti 2*p* signal position were observed during further treatments. Moreover, all Ti 2*p* doublets can be perfectly reproduced by a single Gaussian/Lorentzian doublet at all reduction steps. Even a sample treatment in pure hydrogen at a temperature of 823 K, extended for 47 min, did not lead to any signal of a titanium species with a lower oxidation number than +4. In order to increase the surface sensitivity to the detection limit discussed at the beginning of this section, XPS spectra were taken both at exit angles of 20° and 60° with respect to the surface normal. The resulting spectra together with the fitted doublets are shown in Fig. 10. In both cases the Ti $2p_{3/2}$ peak has a binding energy of 459.4 eV and represents

Ti^{4+} . Both spectra show the same spin-orbit splitting of 5.7 eV and widths (FWHM) (1.4 eV at the 3/2- and 2.3 eV at the 1/2-signal). Even during these severe treatment conditions, no Ti^{3+} or titanium species with lower oxidation numbers are formed.

Depending on the model used for the calculation of the electron mean free path, the maximum amount of Ti^{3+} in the first atomic layer according to this result is determined to 7.4 % (SD) and 4.4 % (TPP). The constant oxidation state of the titanium oxide films is also reflected in the constant Ti/O ratio over the temperature range of the experiments. In Fig. 11, the Ti/O intensity ratios are plotted against the reduction temperature. After the first reduction step, where the rhodium oxide is reduced to rhodium metal, the Ti/O ratios change only with a slope of $1.4 \cdot 10^{-4}$ and $9.5 \cdot 10^{-5}$ for the two series and can be regarded as constant within the limits of the experimental errors. The intensity ratios for the untreated samples (filled symbols in Fig. 11) are considerably lower due to the oxidized rhodium metal at the surface. The reasons for the deviation of the ratio from the expected value of 0.5 for TiO_2 (the experimental ratios are 0.38 and 0.39 for the two series) are first due to the incomplete consideration of the Ti signals. For the ratio, several shake-up signals at higher binding energies than the Ti 2*p* doublet were neglected and only the integral over the energy range covering the 2*p* peak s is used. Secondly, the area detected by the analyzer is larger than the sample size. Contributions from the sample holder to the photoelectron intensities are therefore unavoidable. Since the holder contains oxygen but no titanium, this, as well as the neglect of the shake-up signals, both lead to an underestimation of the Ti/O intensity ratio, compared with the stoichiometric value of 0.5. However, since the XPS spectra only show Ti^{4+} and the additional characterization methods (in this case LRS) give no indication for further titanium oxide modifications, the stoichiometry of TiO_2 for the oxide film is assumed. The constant Ti/O ratio over the whole temperature range covered in the experiments shows that the reduction treatment does not lead to a change in the stoichiometry of the oxide film.

The development of the Ti/Rh XPS intensity ratio with reduction temperature is shown in Fig. 12 for the two treatment series. The first series (square symbols) shows the same development as measured by AES and ISS (Fig. 4) in the low-pressure experiments. The intensity ratio vs. reduction temperature is indicated by the filled symbols and increases slowly between the untreated sample (data point at 300 K) and the 753 K reduction. Following the 823 K reduction, the Ti/Rh ratio shows again a considerable increase. Between the untreated and at 823 K reduced sample the ratio

increases by a factor of about 40. This increase is comparable to the AES results after high-temperature reduction of a Rh/TiO_2 model catalyst at 873 K in vacuum. The large increase of the ratio takes place above 750 K in both experiments. However, the second treatment series (circled symbols) at ambient pressure shows an increase in the Ti/Rh lower by about one order of magnitude, after the 823 K reduction. The difference between the two experimental sequences lies in the overall time at elevated temperatures. Both the sample temperature and the duration of the reduction experiments influence the final Ti/Rh ratio. This is indicated by plotting the ratios vs. a figure of merit H, which considers these two parameters $\left(H = \frac{\text{Reduction Temperature} \times \text{Reduction Time}}{1000}\right)$. Since the first series consists of a greater number of treatments (see Table 3), the value of H is largest for the 823 K treatment of the first experiment. The final reduction step of series 2 only reaches $H = 81$ and the intensity ratio for this number corresponds very well with the intensity ratio of series 1 at this value for H.

4. Summary

Rh/TiO_2 and Rh/Al_2O_3 model catalysts with a Rh coverage of the order of one monolayer were specially prepared and well characterized with respect to thickness, structure and morphology by a variety of surface science techniques. The TiO_2 support layers produced by anodic oxidation to a thickness between 7 nm and 250 nm were completely transformed into the anatase modification by the applied calcination. The Al_2O_3 supports had a thickness of about 20 nm of γ-Al_2O_3. Depth profiling of the Rh/TiO_2 system exhibited complete encapsulation of Rh particles by titania after heating in 10^{-4} hPa H_2 to temperatures above 773 K. This was accompanied by a drastic reduction of its CO adsorption capacity and thus the typical features of strong metal-support interaction (SMSI effect) were observed. No reduced Ti species (e.g. Ti^{3+}) could be observed in our case. This could be related to interactions with the relatively thick oxide layer produced by anodic oxidation. In a different study [34] thin titania layers evaporated onto a Mo support showed the appearance of Ti^{3+} after similar treatments. The amount of Ti species covering the initial Rh surface layer depends on the combined value of temperature times reduction time. The alumina-supported systems showed no such signs of encapsulation , just an interdiffusion of surface layers and support. The study demonstrates the usefulness of model catalysts to which an appropriate variety of surface science techniques can be applied to provide the required characterization of the model systems and the reaction processes on their surfaces.

Acknowledgements

This work was stimulated by Helmut Knözinger in his quest to apply surface physics techniques in the field of catalysis to elucidate mechanisms which cannot be investigated in the complex world of real catalysts. We are grateful for many productive years of collaboration and joyfully dedicate this article to him on the occasion of his 75th birthday.

The authors are grateful for support with the XRD measurements by H.E. Göbel and with the LRS measurements by G. Mestl and D. Spielbauer. Part of this work was carried out under the framework of Sonderforschungsbereich 338 of the Deutsche Forschungsgemeinschaft.

References

[1] G.-M. Schwab and H. Schultes, Z. Phys. Chem. B 9 (1930) 265.

[2] G.-M. Schwab, Adv. Catal. 27 (1978) 1.

[3] S.J. Tauster and S.C. Fung, J. Catal. 55 (1978) 29.

[4] S.J. Tauster, S.C. Fung, and R.L. Garten, J. Am. Chem. Soc. 100 (1978) 170.

[5] S.J. Tauster, S.C. Fung, R.T.K. Baker, and J.A. Horsley, Science 211 (1981) 1121.

[6] G.L. Haller and D.E. Resasco, Adv. Catal. 36 (1989) 173.

[7] M. Boudart and G. Djéga-Mariadassou, *Kinetics of Heterogeneous Catalytic Reactions* (Princeton University Press, Princeton, New Jersey, 1984).

[8] R.T.K. Baker, E.B. Prestridge, and R.L. Garten, J. Catal. 56 (1979) 390.

[9] R.T.K. Baker, E.B. Prestridge, and R.L. Garten, J. Catal. 59 (1979) 293.

[10] J.A. Horsley, J. Am. Chem. Soc. 101(11) (1979) 2870.

[11] B.-H. Chen and J.M. White, J. Phys. Chem. 87 (1983) 1327.

[12] N.K. Ray and A.B. Andersen, Surf. Sci. 125 (1983) 803.

[13] M.S. Spencer, J. Phys. Chem. 88 (1984) 1046.

[14] T. Huizinga, H.F.J. van T'Blik, J.C. Vis, and R. Prins, Surf. Sci. 135 (1983) 580.

[15] D.J. Dwyer, S.D. Cameron, and J. Gland, Surf. Sci. 159 (1985) 430.

[16] C.S. Ko and R.J. Gorte, Surf. Sci. 161 (1985) 597.

[17] K.J. Williams, M. Salmeron, A.T. Bell, and G.A. Somorjai, Surf. Sci. 204 (1988) L745.

[18] M.E. Levin, M. Salmeron, A.T. Bell, and G.A. Somorjai, Surf. Sci. 169 (1986) 123.

[19] M.E. Levin, M. Salmeron, A.T. Bell, and G.A. Somorjai, J. Chem. Soc., Faraday Trans. I 83 (1987) 2061.

[20] M.E. Levin, M. Salmeron, A.T. Bell, and G.A. Somorjai, J. Catal. 106 (1987) 401 .

[21] M.E. Levin, M. Salmeron, A.T. Bell, and G.A. Somorjai, Surf. Sci. 195 (1988) 429.

[22] M.E. Levin, K.J. Williams, M. Salmeron, A.T. Bell, and G.A. Somorjai, Surf. Sci. 195 (1988) 341.

[23] A.D. Logan, E.J. Braunschweig, A.K. Datye, and D.J. Smith, Langmuir 4 (1988) 827.

[24] M.-H. Yao, Proc. 51th Annual Meeting of the Microscopy Society of America, San Francisco Press, San Francisco, Ed. G.W. Bailey and C.L. Rieder (1993) 734.

[25] R. Lamber and G. Schulz-Eklhoff, Ber. Bunsenges. Phys. Chem. 95 (1991) 1479.

[26] H.R. Sadeghi and V.E. Henrich, J. Catal. 87 (1984) 279.

[27] J.-M. Pan, B.L. Maschhoff, U. Diebold, and T.E. Madey, J. Vac. Sci. Technol. A 10 (1992) 2470.

[28] D.N. Belton, Y.-M. Sun, and J.M. White, J. Phys. Chem. 88 (1984) 1690.

[29] D.N. Belton, Y.-M. Sun, and J.M. White, J. Phys. Chem. 88 (1984) 5172.

[30] D.N. Belton, Y.-M. Sun, and J.M. White, J. Am. Chem. Soc. 106 (1984) 3059.

[31] Y.-M. Sun, D.N. Belton, and J.M. White, Prepr.-Am. Chem. Soc., Div. Pet. Chem. 29(3) (1984) 749.

[32] D.N. Belton, Y.-M. Sun, and J.M. White, J. Catal. 102 (1986) 338.

[33] V. Anděra, Appl. Surf. Sci. 51 (1991) 1.

[34] E. Labich, S.and Taglauer and H. Knözinger, Topics in Catal. 14 (2001) 153.

[35] B.A. Sexton, A.E. Hughes, and K. Foger, J. Catal. 77 (1982) 85.

[36] A.K. Singh, N.K. Pande, and A.T. Bell, J. Catal. 94 (1985) 422.

[37] M.C. Muñoz, A.R. Gonzáles-Elipe, G. Munuera, J.P. Espinós, and V. Rives-Arnau, Spectrochimica Acta A 43(12) (1987) 1599.

[38] T. Huizinga and R. Prins, J. Phys. Chem. 85 (1981) 2156.

[39] J.C. Conesa and J. Soria, J. Phys. Chem. 86 (1982) 1392.

[40] S.J. DeCanio, J.B. Miller, J.B. Michel, and C. Dybowski, J. Phys. Chem. 87 (1983) 4619.

[41] V. Vishwanathan, J. Chem. Soc. Chem. Commun. (1989) 848.

[42] V. Vishwanathan and S. Narayanan, Catal. Lett. 21 (1993) 183.

[43] R. Burch and A.R. Flambard, J. Chem. Soc. Chem. Commun. (1981) 965.

[44] V. Vishwanathan and S. Narayanan, J. Chem. Soc. Chem. Commun. (1988) 1233.

[45] F.M. Dautzenberg and H.B.M. Wolters, J. Catal. 51 (1978) 26.

[46] G.J. Den Otter and F.M. Dautzenberg, J. Catal. 53 (1978) 116.

[47] J.A. Cairns, J.E.E. Baglin, G.J. Clark, and J.F Ziegler, J. Catal. 83 (1983) 301.

[48] K. Tamura and Y. Nihei, J. Catal. 115 (1989) 273.

[49] J.G. Chen, M.L. Colaianni, P.J. Chen, J.T. Jr. Yates, and G.B. Fisher, J. Phys. Chem. 94 (1990) 5062.

[50] S.M. McClure, M. Lundwall, F. Yang, Z. Zhou, and D.W. Goodman, J. Phys.: Condens. Matter 21 (2009) 474223.

[51] S.A. Stevenson, J.A. Dumesic, R.T.K. Baker, and E. Ruckenstein, *Metal-Support Interactions in Catalysis, Sintering, and Redispersion* (Van Nostrand Reinhold's Catalysis Series, New York, 1987).

[52] G. Ertl, H Knözinger, F. Schüth, and J. Weitkamp (Eds.), *Handbook of Heterogeneous Catalysis* (Wiley-VCH, Weinheim, 2008), 2nd edition.

[53] Ch. Linsmeier, H. Knözinger, and E. Taglauer, Nucl. Instrum. Methods B 118 (1996) 533.

[54] W. Herrmann, Wiss. Veröff. Siemens-Werkst. Sonderh. 199 (1940) 88.

[55] A. Aladjem, *Anodic Oxidation of Titanium and its Alloys*, Technical report, Israel Atomic Energy Commission (1972).

[56] W. Walkenhorst, Naturwiss. 12 (1947) 373.

[57] D.L. Cocke, E.D. Johnson, and R. P. Merrill, Catal. Rev. - Sci. Eng. 26 (1984) 163.

[58] S. Tajima, Adv. Corros. Sci. Technol. 1 (1970) 229.

[59] Y. Serruys, T. Sakout, and D. Gorse, Surf. Sci. 282 (1993) 279.

[60] D. Hönicke, Appl. Catal. 5 (1983) 179.

[61] F. Kover and J. Musselin, Thin Solid Films 2 (1968) 211 .

[62] H.E. Göbel, Adv. X-Ray Anal. 25 (1983) 315.

[63] G. Debras and G. Deconninck, J. Radioanal. Chem. 38 (1977) 193.

[64] G. Amsel and D. Samuel, Anal. Chem. 39 (1967) 1689.

[65] D.R. Lide (Ed.), *CRC Handbook of Chemistry and Physics* (CRC Press, Boca Raton, 1993), 74st edition.

[66] D. Mehl, Diploma Thesis, Technische Universität München (1988).

[67] H.H Brongersma, M. Draxler, Ridder M. de, and P. Bauer, Surf. Sci. Reports 62 (2007) 63.

[68] K. Josek, Ch. Linsmeier, H. Knözinger, and E. Taglauer, Nucl. Instrum. Methods B 64 (1992) 596.

[69] Ch. Linsmeier, H. Knözinger, and E. Taglauer, Surf. Sci. 275 (1992) 101.

[70] G. Johansson, J. Hedman, A. Berndtsson, M. Klasson, and R. Nilsson, J. Electron Spectrosc. Relat. Phenom. 2 (1973) 295.

[71] B.J. Lindberg, K. Hamrin, G. Johansson, U. Gelius, A. Fahlman, C. Nordling, and K. Siegbahn, Physica Scripta 1 (1970) 286.

[72] G. Malmsten, I. Thorén, S. Högberg, J.-E. Bergmark, S.-E. Karlsson, and E. Rebane, Physica Scripta 3 (1971) 96.

[73] D.A. Shirley, Phys. Rev. B 5 (1972) 4709.

[74] D.M. Proctor, A..and Hercules, Appl. Spectroscopy 38(4) (1984) 505.

[75] S.K. Sen, J. Riga, and J. Verbist, Chem. Phys. Lett. 39 (1976) 560.

[76] U. Balachandran and N.G. Eror, J. Solid State Chem. 42 (1982) 276.

[77] R.J. Nemanich, C.C. Tsai, and G.A.N. Connell, Phys. Rev. Lett. 44 (1980) 273.

[78] P.A. Redhead, Vacuum 12 (1962) 203.

[79] D.G. Castner, B.A. Sexton, and G.A. Somorjai, Surf. Sci. 71 (1978) 519.

[80] L.H. Dubois, P.K. Hansma, and G.A. Somorjai, Appl. Surf. Sci. 6 (1980) 173.

[81] R.W. McCabe, R.K. Usmen, K. Ober, and H.S. Gandhi, J. Catal. 151 (1995) 385 .

[82] H. Knözinger and E. Taglauer, Catalysis 10 (1993) 1.

[83] S.H. Overbury, P.A. Bertrand, and G.A. Somorjai, Chem. Rev. 75 (1975) 547.

[84] A.R. Miedema, Z. Metallkunde 69 (1978) 455.

[85] W. Göpel, J.A. Anderson, D. Frankel, M. Jaehnig, K. Phillips, J.A. Schäfer, and D. Rocker, Surf. Sci. 139 (1984) 333.

[86] M.P. Seah and W.A. Dench, Surf. Interface Anal. 1 (1979) 2.

[87] M.P. Seah, Surf. Interface Anal. 9 (1986) 85.

[88] S. Tanuma, C.J. Powell, and D.R. Penn, Surf. Interface Anal. 11 (1988) 577.

[89] S. Tanuma, C.J. Powell, and D.R. Penn, Surf. Interface Anal. 17 (1991) 911.

[90] S. Tanuma, C.J. Powell, and D.R. Penn, Surf. Interface Anal. 17 (1991) 927.

[91] W. P. A. Jansen, J. Beckers, J. C. v. d. Heuvel, A. W. Denier v. d. Gon, A. Bliek, and H. H. Brongersma, J. Catal. 210 (2002) 229 .

[92] J.P. Contour, G. Mouvier, M. Hoogewys, and C. Leclere, J. Catal. 48 (1977) 217.

[93] Y. Okamoto, N. Ishida, T. Imanaka, and S. Teranishi, J. Catal. 58 (1979) 82.

[94] V.I. Nefedov, M.N. Firsov, and I.S. Shaplygin, J. Electron Spectrosc. Relat. Phenom. 26 (1982) 65.

[95] J.F. Moulder, W.F. Strickle, P.E. Sobol, and K.D. Bomben, *Handbook of X-ray Photoelectron Spectroscopy* (Ed.: J. Chastain, Perkin-Elmer Corp., Minnesota, 1992).

[96] R. Nyholm and N. Mårtensson, J. Phys. C: Solid State Physics 13 (1980) L279.

[97] S.P. Kowalczyk, L. Ley, R.L. Martin, F.R. McFeely, and D.A. Shirley, Faraday Discuss. Chem. Soc. 60 (1975) 7.

Table 1: Oxide film thicknesses, measured by NRA. The ranges indicate the extreme values measured at several different samples. Note (1): This is the expected thickness of the natural air oxide [55].

Oxide film	nominal thickness after anodization [nm]	measured thickness [nm]
Al_2O_3 dried	14.0	21.7
Ti air oxide	7.0 (1)	$7.1 \cdots 8.5$
TiO_2 dried	300.0	225.0
TiO_2 dried	30.0	$236 \cdots 26.5$
TiO_2 calcined	30.0	$54.9 \cdots 83.4$

Table 2: Rhodium adlayer thicknesses n_{Rh}, measured by RBS. The thicknesses are calculated from the areal densities by using the Rh bulk density. Several measurements across the samples show a homogeneous metal distribution over the model catalysts. However, the measured thickness differs from the nominal value, recorded with a quartz crystal microbalance.

Sample	nominal Rh loading [ML]	n_{Rh} $[10^{15}$ atoms/cm$^2]$	d_{Rh} [nm]	d_{Rh} [ML]
Rh/Al_2O_3 calcined	1.0	1.72	0.24	0.88
		1.56	0.21	0.79
Rh/Al_2O_3 dried	1.0	1.57	0.22	0.80
		1.52	0.21	0.77
TiO_2 calcined	0.0	0.032	0.004	0.02
		0.015	0.002	0.01
		0.057	0.008	0.03
Rh/TiO_2 calcined	1.0	1.394	0.192	0.71
		1.313	0.181	0.67
		1.323	0.182	0.68
Rh/TiO_2 dried	1.0	0.934	0.129	0.48
		0.866	0.119	0.44
		0.893	0.123	0.46
		0.838	0.116	0.43

Table 3: XPS binding energies (BE) and peak widths (FWHM) of the Rh/TiO_2 model catalysts in the two reduction series, taken after treatments under the indicated conditions, at ambient pressure.

Sample Treatment	Rh $3d_{5/2}$		Ti $2p_{3/2}$	
	BE [eV]	FWHM [eV]	BE [eV]	FWHM [eV]
Series 1				
as introduced	308.8	2.5	458.5	1.5
603 K, 15 min, 1.5 % H_2	307.7	1.4	459.3	1.4
683 K, 15 min, 1.5 % H_2	307.5	1.5	459.2	1.4
753 K, 15 min, 1.5 % H_2	307.2	1.4	459.2	1.4
683 K, 30 min, 100 % H_2	307.1	1.4	459.1	1.4
753 K, 65 min, 100 % H_2	306.9	1.4	459.1	1.4
823 K, 30 min, 100 % H_2	307.0	1.7	459.1	1.4
Series 2				
as introduced	308.9	2.7	458.6	1.6
603 K, 15 min, 5 % H_2	307.6	1.4	459.1	1.4
683 K, 16 min, 5 % H_2	307.6	1.4	459.4	1.4
753 K, 15 min, 5 % H_2	307.7	1.4	459.4	1.4
753 K, 15 min, 100 % H_2	307.4	1.4	459.5	1.4
823 K, 47 min, 100 % H_2	307.4	1.5	459.5	1.4

Figure 1: Diffraction patterns of two TiO_2 films. The film leading to pattern a has a nominal oxide thickness of 30.0 nm, the sample of pattern b has a nominal thickness of 300.0 nm. Both are calcined at 623 K and show the diffraction signals of anatase. With thin film, the titanium metal signal dominates, whereas in the pattern of the thick film both TiO_2 and Ti metal contribute to the same amount.

Figure 2: Raman spectra of two TiO_2 films. The spectra (a) and (b) are both measured at a sample with a nominal oxide thickness of 30.0 nm, after drying in air (a) and after calcination at 770 K (b). The line at 1057 cm^{-1} is a plasma line from the Ar^+ laser, used for calibration. Spectrum (c) is taken from a TiO_2 film with a nominal thickness of 300.0 nm. The film is also calcined at 580 K. Both oxide films show only signals typical for anatase.

Figure 3: Normalized ISS signals of Rh, O, and Ti of a Rh/TiO_2 model catalyst after the indicated reactive treatment at 573 K (left axis labels) and 773 K (right axis labels). The change in these depth profiles after the high temperature treatment clearly shows the encapsulation of the Rh film by titania species.

Figure 4: Intensity ratios of a Rh/TiO_2 model catalyst before and after reductive treatments at low pressures, measured by AES and ISS. For the ISS data, the intensities after a bombardment with $3 \cdot 10^{16}$ He^+ cm^{-2} are used. The Ti LMM and Rh MNN signals are used for the AES intensity ratio. Both techniques demonstrate the encapsulation of the surface Rh by titanium species.

Figure 5: CO desorption spectra from a Rh/TiO_2 model catalyst as prepared (after applying a gentle cleaning procedure, see text) and after a HTR treatment at 830 K. Both spectra are measured after exposure to 40 L CO.

Figure 6: Normalized ISS signals of Rh, O, and Al of a Rh/Al_2O_3 model catalyst after thermal treatments at 603, 753 and 823 K. The depth profiles show no indication for an encapsulation of rhodium by support material.

Figure 7: XPS spectra of the Ti 2p region, measured at a 3.0 nm Rh/TiO_2 model catalyst before (a) and after (b) bombardment with $1.11 \cdot 10^{16}$ Ar^+ cm^{-2} at an energy of 2 keV. Spectrum (a) is fitted with a single doublet for Ti^{4+}, spectrum (b) with two doublets for Ti^{4+} and Ti^{3+}, respectively.

Figure 8: Comparison of a measured Ti^{4+} signal of a Rh/TiO_2 model catalyst (data points) with calculated XPS titanium peaks (solid lines) with Ti^{3+} fractions of 0 %, 0.5 %, 1 % and 2 % in the first atomic layer. The detection limit for Ti^{3+} with the applied method lies between 1 and 2 %.

Figure 9: XPS Rh 3d spectra of a series of reduction treatments carried out for a Rh/TiO_2 model catalyst with a nominal metal loading of 1 ML. The reduction temperatures are indicated, further parameters are stated in Table 3.

Figure 10: XPS Ti $2p$ spectra of a Rh/TiO_2 model catalyst after a 823 K high-temperature reduction in pure hydrogen for 47 min. The angle denotes the analyzing angle with respect to the surface normal of the sample. In both cases, the experimental data points can be fitted perfectly by only one doublet.

Figure 11: XPS intensity ratios of the Ti $2p$ and O $1s$ signals after several reduction treatments of Rh/TiO_2 model catalysts at ambient pressure. The circles and diamonds represent two different experiments. For the calculation of the straight lines only the open symbols were considered.

Figure 12: XPS intensity ratios of the Ti $2p$ and Rh $3d$ signals after several reduction treatments at ambient pressure for two experimental series represented by circles and squares, respectively. For details see text. The solid symbols refer to the lower abscissa where the treatment temperature is plotted. The open symbols represent the same sample treatments, however, plotted against the product of reduction temperature and treatment time. This number represents a figure of merit which indicates not only the sample temperature, but also the total time the sample has been treated at elevated temperatures.

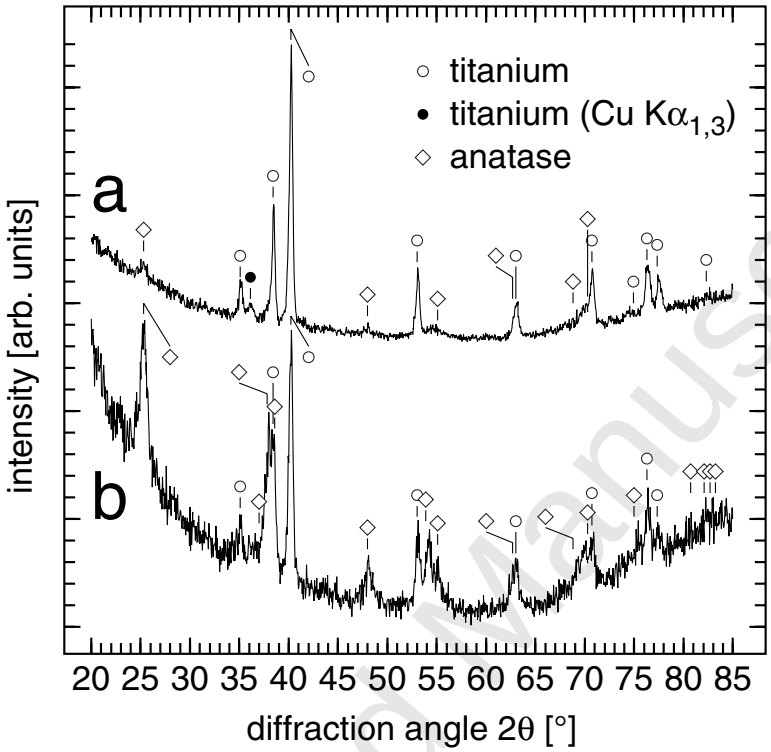

Fig. 1

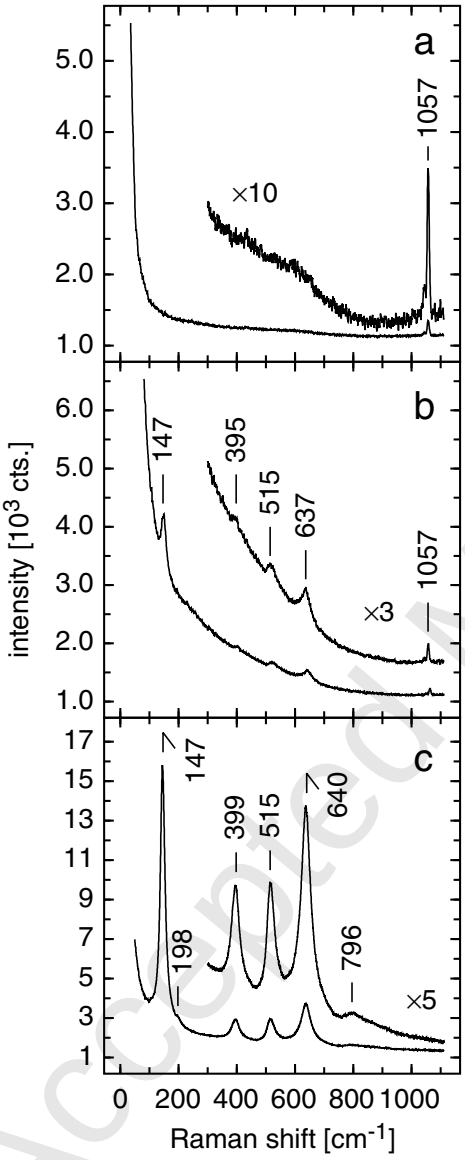

Fig. 2

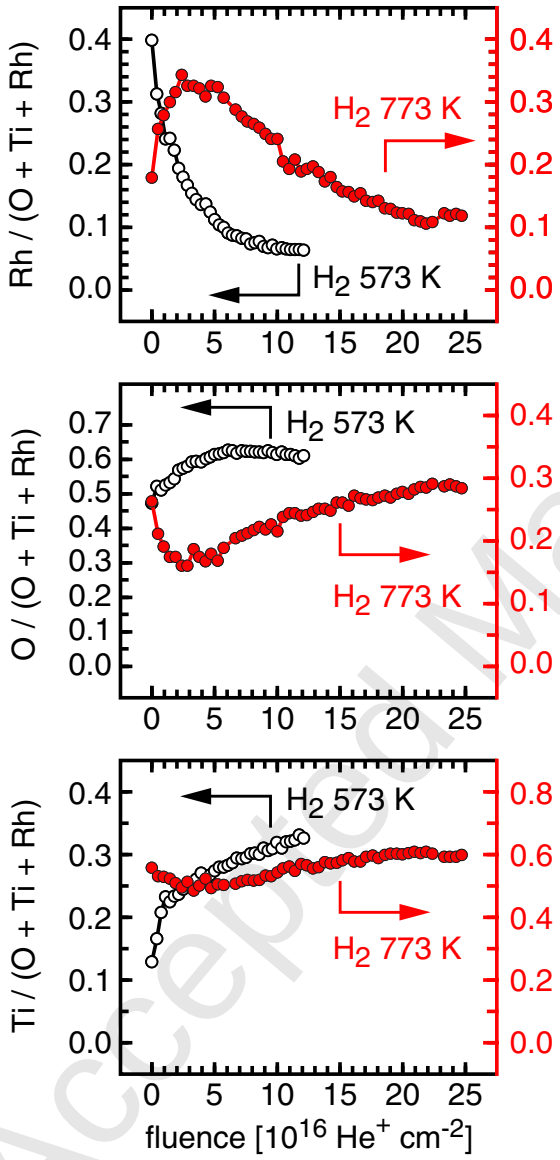

Fig. 3

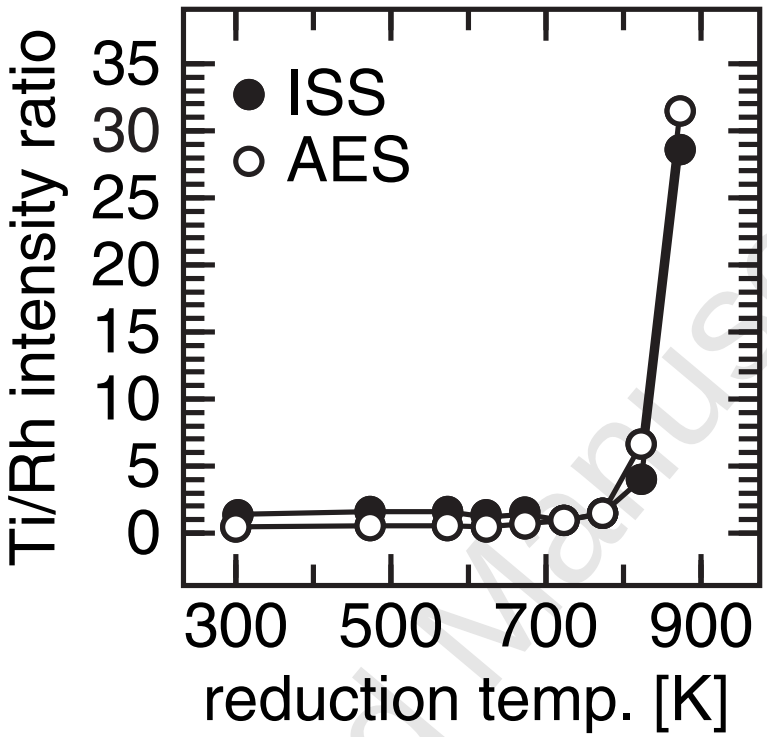

Fig. 4

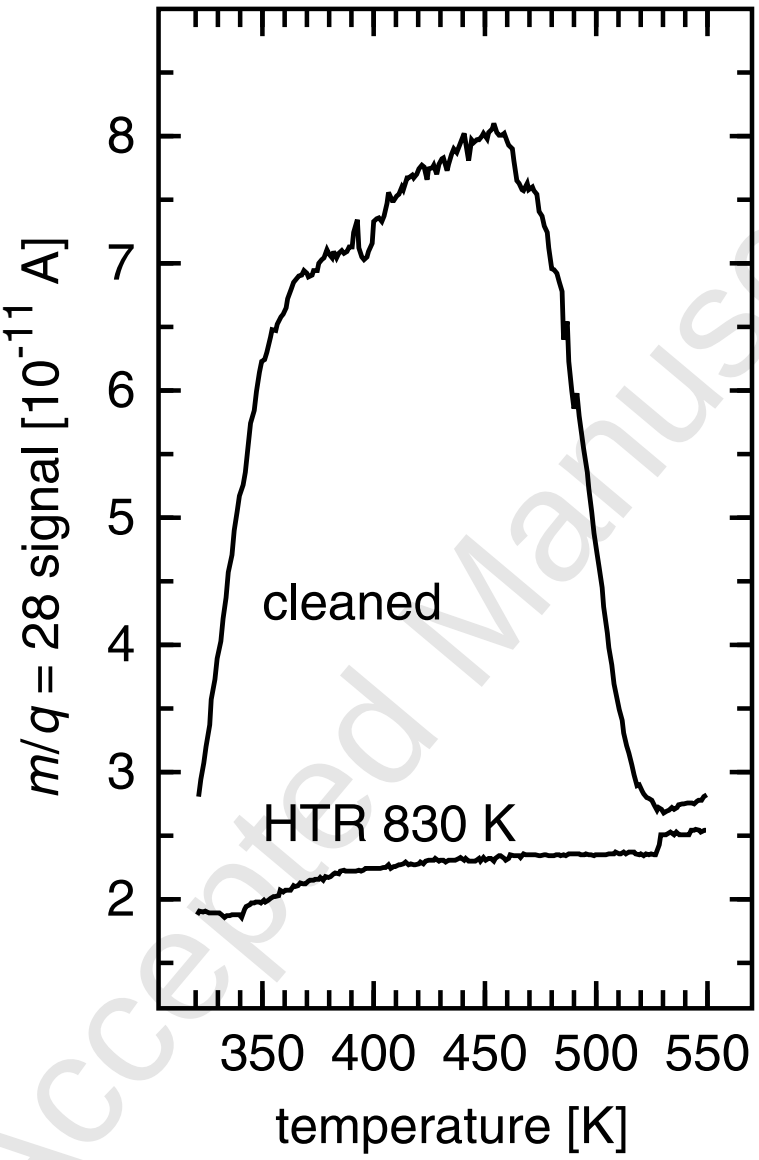

Fig. 5

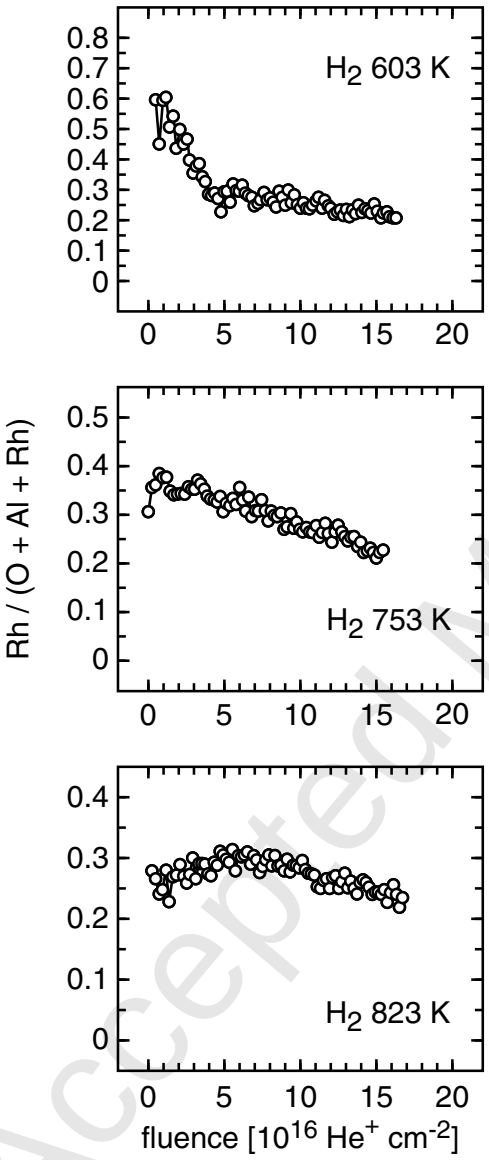

Fig. 6

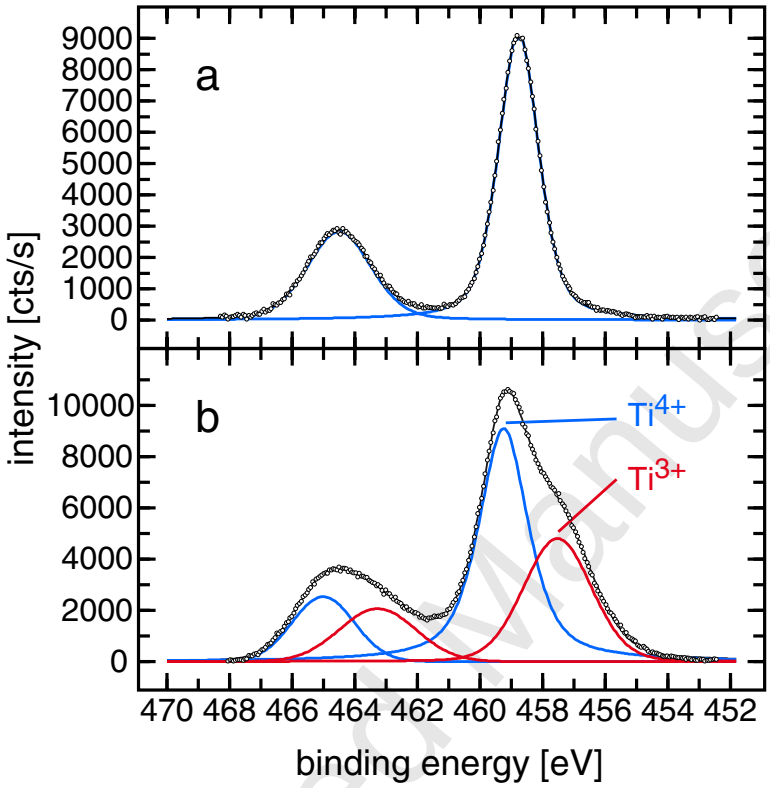

Fig. 7

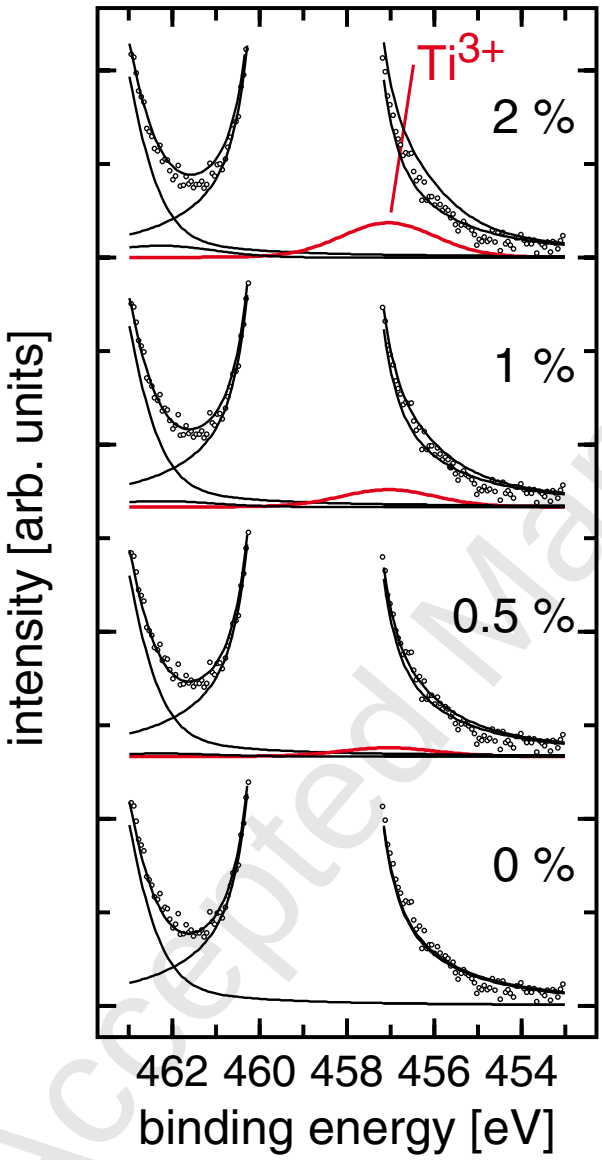

Fig. 8

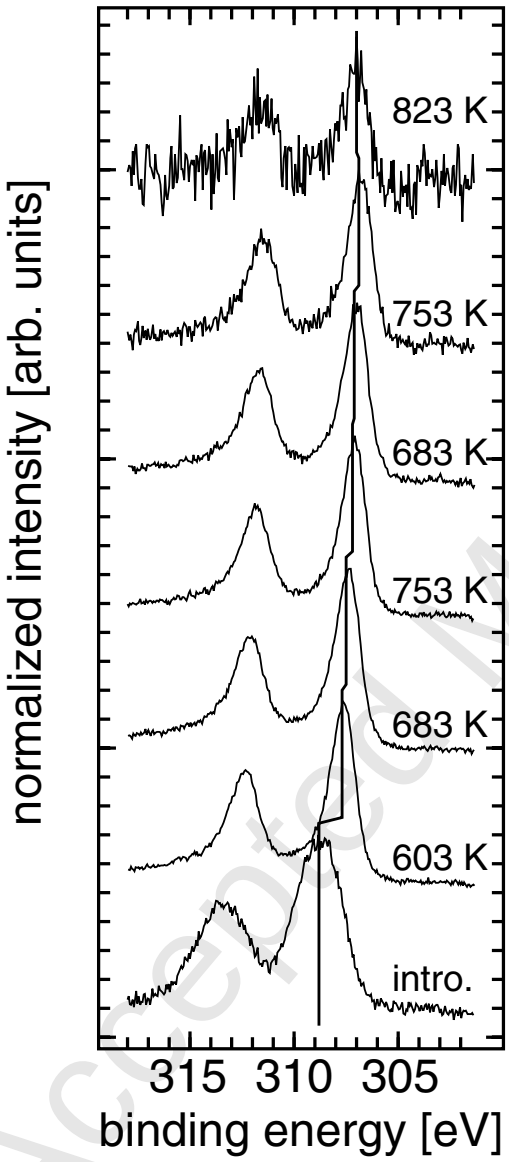

Fig. 9

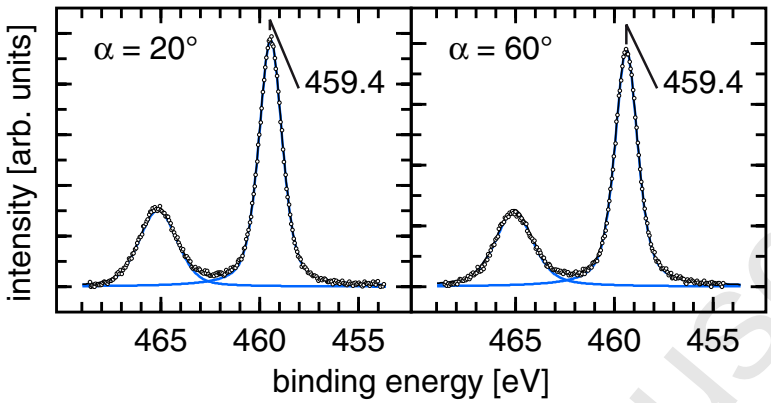

Fig. 10

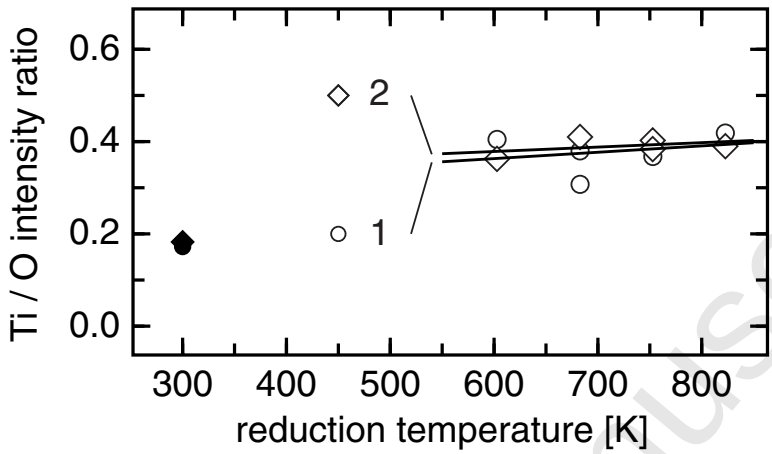

Fig. 11

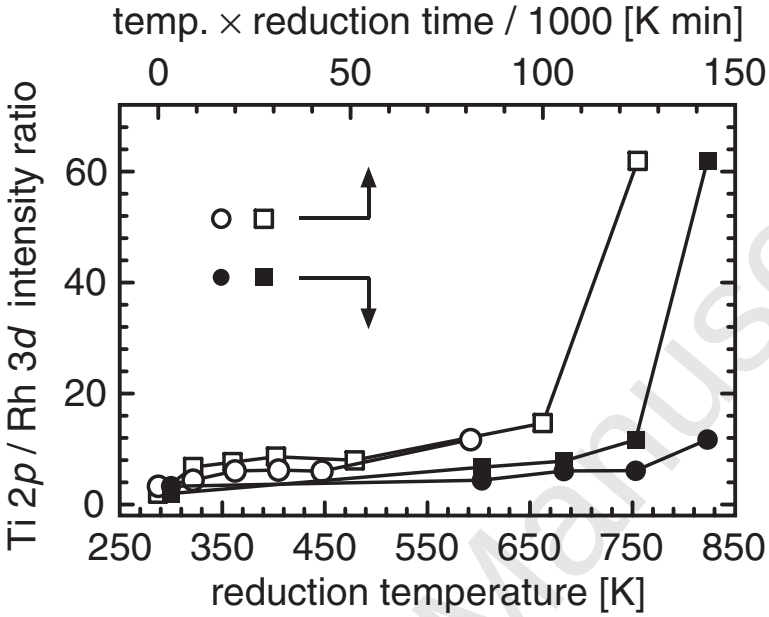

Fig. 12

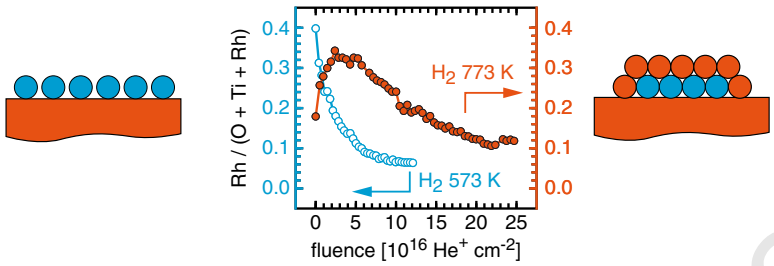

Fig. Graphical abstract